AIAA SciTech
13-17 January 2014, National Harbor, Maryland
52nd Aerospace Sciences Meeting

Near-field Pressure and Far-field Acoustic Response of Forced High-Speed Jets

M. Crawley[1†], A. Sinha[2¶] and M. Samimy[1§]
[1]*Aerospace Research Center, The Ohio State University, Columbus, OH, USA*
[2]*Department of Mechanical Engineering, California Institute of Technology, Pasadena, CA, USA*

The near-field pressure of an unheated, Mach 0.9 jet with a Re_D of 6.2x10^5 excited by plasma actuators has been investigated in order to evaluate the hydrodynamic and acoustic response of the jet, and the link between the two. Simultaneous acquisition of the far-field acoustic, the near-field pressure, and the actuation phase enables the use of phase-averaging of the pressure and acoustic signals and space-time correlations between the near field and the far field. By applying a filter in the frequency-wavenumber space, the near-field pressure is decomposed into its constitutive hydrodynamic and acoustic components. Finally, wavelet analysis is utilized to assess the decomposed fields in the time domain. Both the hydrodynamic and acoustic response to forcing for $St_{DF} < 0.50$ are found to follow a quasi-linear interaction model, in which the response to periodic forcing can be well predicted by a simple linear superposition of the impulsive response. Measurements of the pressure fluctuations and correlations to the far-field aft angle display an upstream shift in the structure saturation point as well as the dominant acoustic source region with increasing forcing frequency. Preliminary investigation in the time-domain found significantly lower temporal coherency of the acoustic response versus the hydrodynamic response; this difference was reduced by periodic forcing.

Downloaded by Mo Samimy on February 3, 2014 | http://arc.aiaa.org | DOI: 10.2514/6.2014-0527

Nomenclature

a_∞	=	Ambient speed of sound (m/s)
k_x	=	Axial wavenumber (rad/m)
D	=	Nozzle exit diameter (m)
U_j	=	Nozzle exit velocity (m/s)
U_c	=	Convective velocity of large-scale structures (m/s)
f	=	Spectral frequency (Hz)
f_F	=	Forcing frequency (Hz)
r	=	Radial coordinate normal to the jet axis (m)
R	=	Distance from near-field microphone to far-field microphone (m)
Re_D	=	Reynolds number based on D and nozzle exit conditions
St_{DF}	=	Forcing Strouhal number ($f_F D/U_j$)

I. Introduction

Acoustic radiation generated by jet engines has long been a concern in the commercial and military aviation industries. The escalating number of flights, encroachment of urban and residential areas near airports, and tightening of environmental regulations have forced airports to introduce costly curfews, surcharges, flight path restrictions, and other measures to reduce noise levels in and around airports. Implementation of flow control strategies, either passive or active, is necessary in order to meet future aircraft noise regulations as well as the performance requirements. Many techniques to reduce the acoustic radiation from high-speed jets using either passive or active modifications to the nozzle have been investigated; however only a passive control, namely chevrons, has been implemented. All active control techniques on the other hand are in various development stages. This is because no consensus has yet formed in the aeroacoustic community over the precise mechanism by which subsonically convecting coherent structures generate sound, despite decades of work, and how to actively control it.

The field of aeroacoustic research was pioneered by Lighthill, who showed that the established governing equations for fluid dynamics could be rearranged into an inhomogeneous wave equation in which a stress tensor (later referred to as Lighthill's stress tensor) is the source[1]. As this acoustic analogy is exact, full knowledge of the

† Graduate Research Assistant, Department of Mechanical and Aerospace Engineering , AIAA Member
¶ Postdoctoral Scholar, AIAA Member
§ Nordholt Professor of Mechanical and Aerospace Engineering, AIAA Fellow, Corresponding Author, Samimy.1@osu.edu

Copyright © 2014 by M. Crawley, A. Sinha, and M. Samimy. Published by the American Institute of Aeronautics and Astronautics, Inc., with permission.

source term would yield an exact solution for the far-field acoustic radiation. However, for jets of practical interest a full description of the source term is not currently available, either experimentally or numerically, forcing researchers to use simplified models. Given the stochastic description of turbulent shear layers commonly held at the time, early work utilized random, uncorrelated eddies as a source model. While this source model, and the resulting U_j^8 power law it produced, found some success, it was shown[2] to be deficient in explaining many aspects of jet noise, in particular the directivity of acoustic radiation in subsonic jets.

Following the discovery of coherent structures in the form of instability waves in turbulent shear layers by Mollo-Christensen[3] and later Crow & Champagne[4], source models of increasing complexity based on coherent eddies have been suggested by researchers. Using conditional averaging, Moore[5] was able to identify waves which were correlated over lengths greater than the local integral turbulence scale. These axially extended waveforms have been identified as having wavepacket characteristics[6], which has led to the frequency-domain description of the large-scale structures. Spatial modulation of the wavepacket was shown to produce the superdirective character of far-field acoustic radiation observed in subsonic jets[7]. (In fact, this modulation is necessary for subsonically convecting structures to radiate to the far field[6].) Similarly, temporal modulation of the wavepacket, in terms of amplitude and envelope, has been shown to improve agreement with numerical results in terms of directivity and amplitude[8,9]. Though significant advancements have been made towards the understanding of aeroacoustic sound generation, more work is necessary in order to fully characterize the salient characteristics of the turbulent eddies in regards to sound production. Control of the development of the shear layer of the jet, and hence the frequency content and phase of the coherent structures, may provide another avenue for investigation of the source mechanism and ultimately noise mitigation.

The Gas Dynamics and Turbulence Laboratory (GDTL) has developed a class of plasma actuators, referred to as localized arc filament plasma actuators (LAFPAs), which can provide excitation signals of high amplitude and high frequency required for control of high Mach number and high Reynolds number jets[10,11]. GDTL has used these actuators for noise mitigation and flow control in Mach 0.9[12,13], Mach 1.3[14-16] and Mach 1.65[17] unheated jets, and has recently expanded the use of LAFPAs to heated jets[18]. A review of the development of LAFPAs and their use in flow control and fluid phenomena research in high speed, high Reynolds number jets, both heated and unheated, can be found in Samimy et al.[19].

More recently, the diagnostic potential of LAFPAs for understanding jet flow phenomena has been explored. Excitation of the flow by LAFPAs results in a definitive spatio-temporal origin to which resulting phenomena can be referenced. The absolute temporal reference afforded by LAFPA excitation provides researchers the ability to investigate the growth, saturation, and decay of structures with high fidelity. Kearney-Fischer et al.[20] investigated Mach wave radiation from heated, high Mach number jets using schlieren imaging phase-locked to LAFPAs, among other data acquisition techniques. Sinha et al.[21] showed the quasi-linearity of large-scale structure interaction through phase-averaging of the near-field pressure in jets forced at low Strouhal numbers ($St_{DF} < 0.5$). Furthermore, the behavior of the seeded structures was found to be well predicted by linear parabolized stability theory. Alkandry et al.[22] and Crawley et al.[23] showed that the coherent large-scale structures produced by the forcing in turn generated coherent radiation to the far field at aft angles. By correlating the near-field pressure and the acoustic far-field, it was shown that the quasi-linear interactions of the structures did not affect the sound source statistics or source region.

In the current work, the range of forcing Strouhal numbers has been increased to provide a more complete characterization of the interaction of the large-scale structures, and their effect on the far-field acoustic radiation. Additionally, the microphone array grid has been extended, which enables the decomposition of the near-field pressure into its hydrodynamic and acoustic constituents via a wavenumber-frequency filtering algorithm. Such a decomposition has been performed previously by other researchers[24]. Inspection of the individual components will yield further insight into the noise source region and ultimately the noise source mechanism or mechanisms.

II. Experimental Methodology

All experiments were conducted at the GDTL within the Aerospace Research Center at the Ohio State University. Compressed, dried, and filtered air is supplied to the facility from two cylindrical storage tanks with a total capacity of 43 m^3 and maximum storage pressure of 16 MPa. The air may be routed through a storage heater (not used in this study), which allows the jet to operate with a stagnation temperature up to 500 °C, before expanding through a nozzle and exhausting horizontally into an anechoic chamber. Opposite the nozzle, a collector accumulates the jet and entrained air from the jet and exhausts it to the outdoors. A schematic of the anechoic chamber can be seen in Figure 1. The dimensions of the chamber are 6.20 m wide by 5.59 m long and 3.36 m tall, with internal wedge-tip to wedge-tip dimensions of 5.14 m by 4.48 m and 2.53 m, respectively. The design of the

Downloaded by Mo Samimy on February 3, 2014 | http://arc.aiaa.org | DOI: 10.2514/6.2014-0527

chamber produces a cutoff frequency of 160 Hz, well below the frequencies of interest. A more detailed description of the GDTL anechoic chamber properties and validation has been given by Hahn[25].

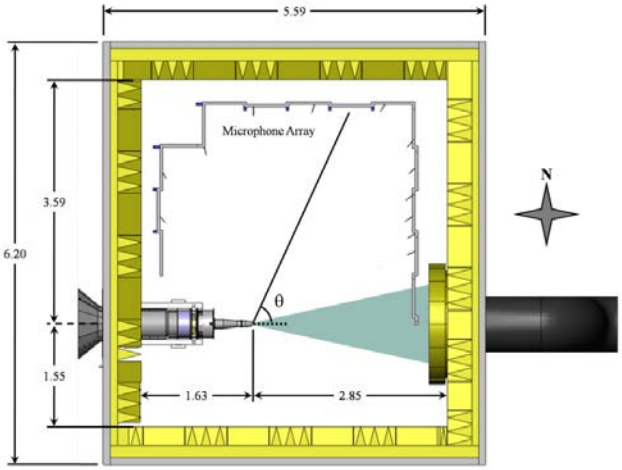

Figure 1: Plan view of the anechoic chamber at the GDTL (dimensions in meters).

For this study a converging, axisymmetric nozzle with exit diameter D of 25.4 mm (1 in.) was used. The internal contour of the nozzle was designed using a fifth order polynomial. The nozzle utilized a thick-lipped design in order to simplify the mounts for the extension, which housed the eight actuators used in this study. For the experiments reported in this paper, the jet was operated at a Mach number (M_j) of 0.90, and with a total temperature ratio of unity. The Reynolds number based on the jet exit diameter was 6.2×10^5; previous investigations using hot-wire anemometry have indicated that the initial shear layer is turbulent for this operating condition with momentum thickness ~0.09 mm and displacement thickness ~1.2 mm[26].

A. Localized Arc Filament Plasma Actuators

Each LAFPA consists of a pair of tungsten pin electrodes, which are placed around the nozzle perimeter 1 mm upstream of the nozzle exit. Eight uniformly spaced actuators are used in this study. The center-to-center spacing between electrode pairs for each actuator is 4 mm. The electrodes are housed in a boron nitride extension attached to the end of the nozzle. A groove with dimensions of 1 mm wide and 0.5 mm deep is machined in the boron nitride, into which the electrode tips protrude, to provide a region of low momentum flow in order to stabilize the plasma arcs. It has been shown that the existence of this groove does not substantially alter the flow field or the control authority of the LAFPAs[27]. A more detailed description of LAFPA characteristics can be found in Utkin et al.[11].

The LAFPAs are energized by a multi-channel, high-voltage plasma power generator capable of simultaneously powering up to eight LAFPAs, which was designed and built in-house at the GDTL. In the second-generation power supply, each individual circuit consists of a switchable capacitor in line with a high voltage transformer; the arcing electrodes are connected to the secondary side of the coil. The capacitor is charged by a 100 V DC power supply when the first switch is closed and the second is opened; at the user-specified time the switches flip and it discharges through the coil. The switches are controlled by a 16-channel digital I/O card and National Instruments' Labview software, operated by a dedicated computer. The plasma generator provides independent control of the frequency, duty cycle/pulse width, and phase of each individual actuator (though not the amplitude). The pulse width was held constant at 7 μs, which was found to be the minimum pulse width at which the actuators consistently arced for all frequencies explored in this study[27]. The circuit is capable of operating at up to 100 kHz, though presently it is limited to 20 kHz due to thermal concerns. In order to improve our understanding of the linear and nonlinear dynamics of the large-scale structure interactions, the range of forcing Strouhal numbers has been expanded to include Strouhal numbers ranging from 0.02 to 0.50; an azimuthal mode of m = 0 was used in all cases.

B. Data Acquisition

Near-field and far-field pressure measurements were acquired simultaneously, using Brüel & Kjær ¼ inch 4939 microphones. The signal from each microphone is band-pass filtered from 20 Hz to 100 kHz using a Brüel & Kjær Nexus 2690 conditioning amplifier, and recorded using National Instruments PXI-6133 A/D boards and LabView software. The microphones are calibrated using a Brüel & Kjær 114 dB, 1 kHz sine wave generator. The frequency response of the microphones is flat up to roughly 80 kHz, with the protective grid covers removed. Voltage signals

Downloaded by Mo Samimy on February 3, 2014 | http://arc.aiaa.org | DOI: 10.2514/6.2014-0527

are collected at 200 kHz with 81920 data points per block; sub-blocks of 8192 data points were used when calculating short-time power spectral densities, resulting in a frequency resolution of 24.4 Hz. Ten blocks were recorded for each case resulting in four seconds of data, which has been found to be sufficient for statistical convergence.

Far-field acoustic pressure is acquired at three polar angles: 30°, 60° and 90°, as measured from the downstream jet axis. The microphones are oriented such that the normal vector from their tips intersects the jet downstream axis at the nozzle exit. The radial distance of the microphones ranges from 101*D* at 30° to 145*D* at 60°. The near-field pressure was acquired using a linear array of sixteen microphones located along the meridional plane of the jet; the spacing varied along the array from 1*D* to 2*D* (Figure 2). The linear array is mounted on a linear traverse system at an angle of 8.6º to the jet axis in order to match the spreading angle of the jet shear layer for this Mach number, as determined via PIV measurements during previous studies[26]. The traverse is controlled using LabView and enables the acquisition of pressure measurements at various radial positions with respect to the jet axis. Initially, the most upstream microphone is positioned at x/D = 1 and r/D = 1.20, to ensure that the microphone tips are outside the mixing layer and do not affect the flow field. For subsequent cases, the microphone array is incremented radially outward by 0.5*D* for a total travel distance of 7*D*, for a total of 15 microphone locations in the radial direction. A schematic of the microphone locations can be found in Figure 2.

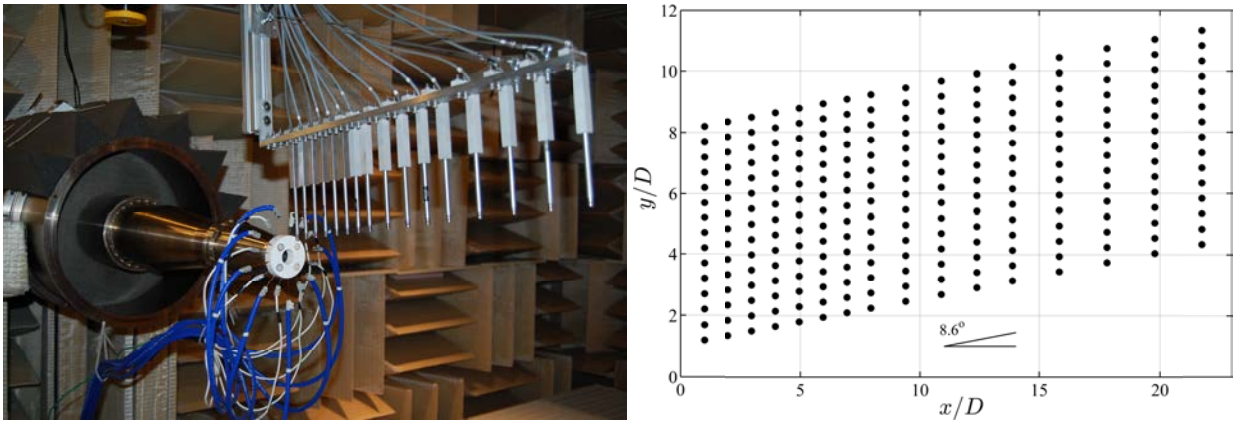

Figure 2: Photograph of anechoic chamber and nozzle, with near-field linear microphone array in foreground (left), schematic of all near-field microphone locations (right).

In the present work, the phase-averaging technique used in Sinha et al.[21] is employed in order to study the evolution of the seeded perturbations, both spatially and temporally. The TTL pulse sequence, which controls the LAFPAs, is supplied to an Agilent 3320A waveform generator. The rising edge of the TTL pulse triggers a sharp drop in the output voltage of the waveform generator, which then ramps back up to the original voltage over a time interval which is shorter than the minimum forcing period. The output from the waveform generator is acquired simultaneously with the near- and far-field pressure signals using the aforementioned National Instruments hardware and software. As the forcing frequency, azimuthal mode, and ramp signal are well defined, this system enables the identification of the zero phase of actuation and hence, the ability to phase-average the pressure signals over the forcing period. This ensures that the seeded perturbations can be readily identified in the noisy flow, as well as allowing pressure signals, which were not recorded simultaneously (i.e. different near-field array positions), to be analyzed concurrently.

Analysis of the near-field response of the forced jet is not immediately straightforward due to acoustic contamination from the actuators themselves[21]. LAFPAs operate on a joule heating principle - the breakdown of the air between the electrodes and the ensuing flow of current results in intense heating of the air. This rapid, localized thermal perturbation produces a compression wave, which excites the shear layer. However, this compression wave is still evident as it travels through the near field. Obviously, this is an undesirable effect, as this actuator self-noise may in some cases obscure the hydrodynamic and acoustic response of the jet. In the present work, the near-field pressure signals have been preprocessed using a continuous-wavelet-based filtering algorithm, which has been specifically designed to remove the actuator self-noise while leaving the signature of the jet response unaltered. For consistency, all results shown have been computed from the filtered, rather than the raw, signals. Further details of the filtering algorithm and sample filtered and raw signals can be found in the references[22].

Downloaded by Mo Samimy on February 3, 2014 | http://arc.aiaa.org | DOI: 10.2514/6.2014-0527

C. Wavenumber-Frequency Filtering

The irrotational near field of the jet comprises both the hydrodynamic footprint of the large-scale structures in the mixing layer as well as acoustic radiation. As has been discussed by numerous other researchers, interpretation of the near-field pressure is hampered by our ignorance of what fluid phenomena are being measured. Recent experiments and analyses[28,29] have shown that the total near field can be thought of as a linear superposition of these two constitutive fields. Therefore, a suitably designed linear filter can, in principle, extract the constitutive fields from the experimentally measured near field. In this work, this decomposition is obtained via a Fourier-based wavenumber-frequency filtering operation computed separately along the microphone array at each radial position. For the jet Mach number explored in this study all hydrodynamic components are expected to have a subsonic convection velocity aligned in the axial direction. On the other hand, acoustic fluctuations will appear either sonic or supersonic along the microphone array, depending on the source location. Hence, the decomposition can be accomplished by setting the filter cutoff based on axial wavenumber to $k_a = \omega/a_\infty$ at each frequency and additional Fourier transforms in space are unnecessary[24]. Therefore, the transformed pressure field is computed as

$$\hat{p}(k_x, \omega) = \frac{1}{2\pi} \iint W_w(x,t) p(x,t) e^{-i(\omega t - k_x x)} dx dt$$

Note that the realities of the physical setup require the transform to actually be computed along the microphone array angle; from this wavenumber the axial wavenumber is then computed. The window function, W_w, is defined as a Tukey window in order to minimize truncation effects as well as distortions to the original signal after the subsequent inverse transforms. To ease in computation of the FFT, the experimental data is interpolated onto a regular grid of spacing $1D$ using a cubic spline. The subsonic and supersonic components are then computed separately as

$$p_c(x,t) = \iint W_c(k_x, \omega) \hat{p}(k_x, \omega) e^{i(\omega t - k_x x)} dk_x d\omega$$

The component weight vector, $W_c \in [0,1]$, is set based on the phase velocity for each k_x, ω pair. Due to the discrete nature of the FFT being performed, an exponential decay about the sonic wavenumber is used, rather than a sharp cutoff. This reduces the effects of the windowing (specifically energy leakage) and decreases 'ringing' in the decomposed waveforms.

III. Results

Examination of the acoustic source dynamics must be preceded by a thorough dissection of the near-field response of the jet to forcing. This will be accomplished first by inspection of the evolution of the phase-averaged waveforms in space and the energy transfer from the near-field to the far-field via two-point correlations. Subsequently, the near-field pressure will be decomposed into its constitutive acoustic and hydrodynamic fields using the wavenumber-frequency filter. These decomposed fields will be investigated using phase-averaging and two-point correlations as well. Finally, details of the noise generation process will be explored using wavelet transforms.

A. Near-field response to forcing

1. Wave component

The hydrodynamic response of the jet to forcing with plasma actuators has been studied in great detail. By decomposing the forced near-field pressure into a wave and residual component[30], Sinha et al[21] showed that each plasma pulse produces a coherent structure that is first amplified as it advects through the mixing layer and later saturates and decays. As the forcing frequency was reduced, the period between successive seeded structures became so great that they evolved independently. In this regime, the response of the jet generating a single coherent structure per actuation, dubbed the 'impulse' or fundamental response, could be studied. It was found that the forcing produced a strong compression wave closely followed by an expansion wave in the irrotational near-field. However, as the forcing frequency was increased, the period between structures is reduced to the point where they begin interacting with each other as they evolve downstream. It was shown[21] that for a certain range of forcing frequencies ($St_{DF} \leq 0.50$ at $x/D = 2$, for example), the structures interact in a quasi-linear manner, insofar as their near-field pressure signatures are concerned. That is, the response of the jet could be well-predicted by a linear superposition of the fundamental response at that particular axial location, repeated at the proper frequency. As the structures are amplifying/decaying as they advect through the mixing layer, the frequency at which the structures begin interacting is dependent on the axial location.

Downloaded by Mo Samimy on February 3, 2014 | http://arc.aiaa.org | DOI: 10.2514/6.2014-0527

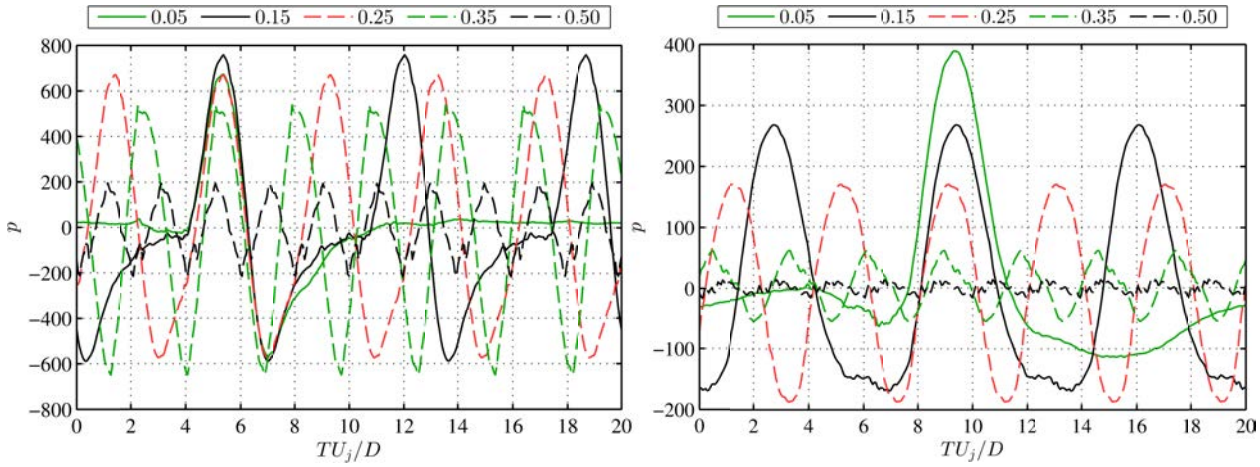

Figure 3: Phase-averaged waveforms for all St_{DF} numbers along the first array position at x/D = 3 (left) and x/D = 6 (right).

This behavior of independent and linear interactions between structures can be observed in Figure 3, where the phase-averaged response of the jet has been plotted along the first microphone array position (closest to the jet shear layer) at two axial locations, x/D = 3 and x/D = 6, for all St_{DF} explored in this study. At the upstream position, the fundamental response of the jet is observed for the two lowest forcing frequencies, St_{DF} = 0.02 and 0.05, as the characteristic period of the compression and expansion waves is much less than the period of forcing. As the forcing frequency is increased, the structures begin interacting linearly. For St_{DF} = 0.15 to 0.25, the magnitudes of the peak and trough are nearly unchanged and the shape is largely unaffected, yet the characteristic period of the response is reduced. Further increases in the forcing frequency, to St_{DF} = 0.35 and 0.50, yields structures for which the amplitude has been significantly reduced, as has the characteristic period. Further downstream, the frequencies at which linear interactions occur have shifted, due to growth of the coherent structures. For the lowest frequency, the fundamental response of the jet is still observed; the waveform still returns to the ambient pressure before the next forcing period. At St_{DF} = 0.05, the structures are just beginning to linearly interact (note that the end of the expansion wave from the previous structure is visible just before the main waveform). Beyond this frequency, the structures undergo significant interaction, with increasing reduction in the peak amplitude and deformation of the waveform shape.

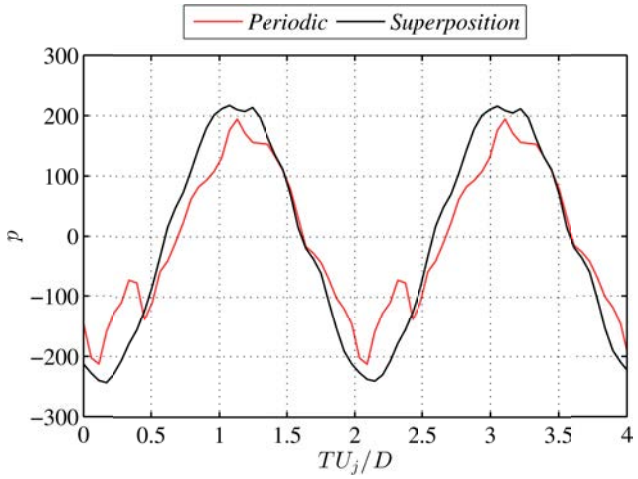

Figure 4: Effect of periodicity of the forcing on the response of the jet at x/D = 3 in which the periodic response at St_{DF} = 0.50 is modeled as a linear superposition of the impulse response at St_{DF} = 0.05.

In Figure 4, the response of the jet at x/D = 3 to forcing at St_{DF} = 0.50 has been reproduced; additionally, a linear superposition of the fundamental response for St_{DF} = 0.05, repeated to match the forcing frequency of St_{DF} = 0.50, has been overlain. Clearly, the quasi-linear interaction model produces close predictions of the waveform amplitude and shape (though not shown here, similar results were found for St_{DF} = 0.25 and 0.35 at this axial location as well

Downloaded by Mo Samimy on February 3, 2014 | http://arc.aiaa.org | DOI: 10.2514/6.2014-0527

as locations further downstream). While some small discrepancies between the periodic and superposition waveforms do exist, for which previous researchers[21] have suggested nonlinearities may be accountable, the near-field hydrodynamic pressure response of the jet is largely governed by linear dynamics over the forcing regime explored in this study.

The growth, saturation, and decay of the large-scale structures generated by forcing can be measured by the mean-square pressure fluctuations along the first array position, shown in Figure 5. In the case of the unforced jet (shown by St_{DF} = 0.00 in the caption), the fluctuations peak at x/D = 5, which is just upstream of the end of the potential core (as determined by previous studies[26]), and slowly decays beyond that point. Forcing at the lowest frequency results in an amplification of the fluctuation energy over nearly the entire domain, though it is most significant near the saturation point. In this case, the saturation point has shifted upstream, to x/D = 4, and displays a slightly sharper peak. Increasing the forcing frequency yields further amplification of the pressure fluctuations as well as an upstream shift in the saturation location. These results are consistent with those of other researchers, who have shown that perturbation of higher frequencies saturate earlier upstream than lower frequencies[31,32]. In this context the sharper peak of the forced results is unsurprising, since a significant portion of the fluctuating energy is being concentrated into one fundamental frequency which saturates at a specific axial location (in the mean) versus the much more broadband energy composition of the natural jet. The change in peak amplitude is not monotonic with forcing frequency; maximum amplification occurs for St_{DF} = 0.25 to 0.35 and decreases quickly for the highest forcing frequency. This corresponds to the well-documented jet column mode forcing response[4].

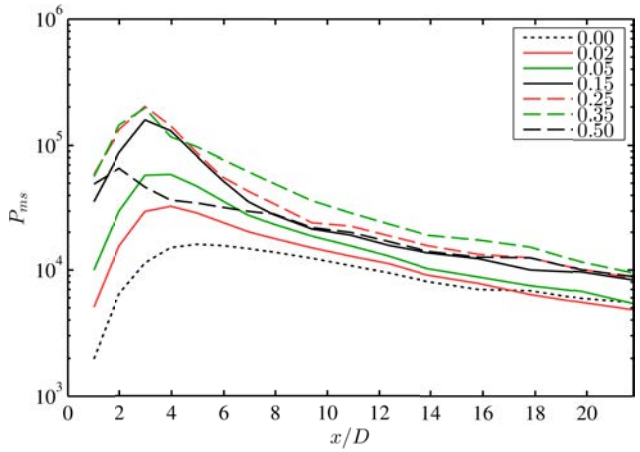

Figure 5: Pressure fluctuation intensity along the first array position for the unforced (indicated as 0.00) and forced jets.

As the array is traversed outwards from the jet shear layer, the dominance of the hydrodynamic signatures of the large-scale structures is reduced, and the behavior of the acoustic response begins to be illuminated. In Figure 6 the phase-averaged waveforms have been plotted for the furthest axial and radial microphone (only four forcing cases are shown for legibility); additionally, the phase-averaged waveforms at the far-field microphone at 30° are shown. In the near field, the fundamental response, comprising a relatively strong expansion wave followed by a relatively strong compression wave, trailed by a weaker set of expansion and compression waves, can be observed for St_{DF} = 0.02 and 0.05. For St_{DF} = 0.15 the primary expansion and compression waves remain nearly unchanged from the fundamental response aside from a slight augmentation of the peak. However due to the periodic forcing, the weaker expansion and compression waves are no longer identifiable, as they're subsumed by the primary waves. At higher St_{DF}, a continuous oscillation between sharp expansion and compression waves is again observed, though both the amplitude and period are reduced from the fundamental response. As before, a linear superposition of the fundamental response can well predict the waveform shape and amplitude at the higher forcing frequencies, though in this case only up to St_{DF} = 0.25. Whether this breakdown in the linear superposition model at the highest forcing frequencies is due to nonlinear behavior or uncertainty in the phase-averaging currently is unknown.

Similarly, in the far field at low polar angles, the fundamental response of the jet can be observed for the lowest two St_{DF}'s. Remarkably, the waveform in the far field is quite similar to that of the near field at far radial and axial positions (though at a much lower amplitude due to inverse-law decay), indicating that the dominant acoustic signature is being captured in the near-field measurement domain. Again, for St_{DF} > 0.25 the amplitude of the compression and expansion waves is significantly reduced. The phase-averaged waveforms were also investigated at polar angles of 60° and 90°; however a clear waveform was not identifiable over the statistical uncertainty inherent

Downloaded by Mo Samimy on February 3, 2014 | http://arc.aiaa.org | DOI: 10.2514/6.2014-0527

in the phase-averaging process. If the forcing is producing coherent radiation to the sideline angles, the amplitude is too low to be observable by phase-averaging.

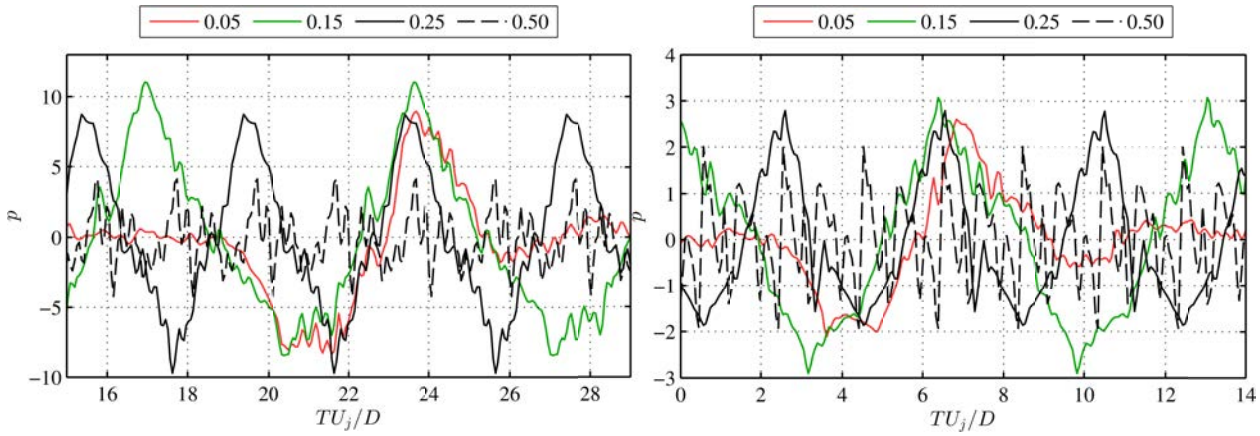

Figure 6: Phase-averaged waveforms at the furthest radial and axial position, corresponding to *x/D* = 21.7, *y/D* = 11.3 (left) and at 30° far-field (right).

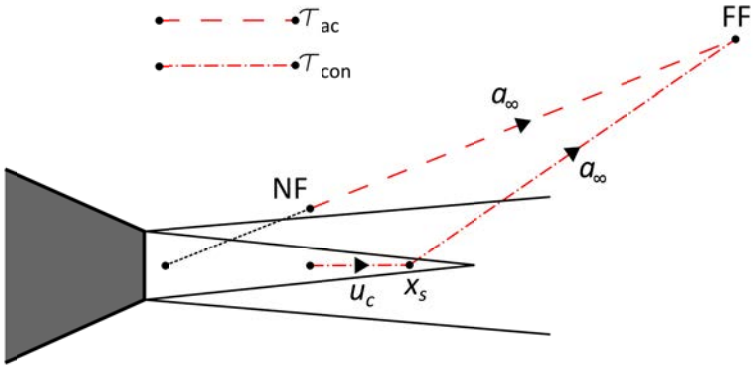

Figure 7: Schematic of propagation paths for expected time of arrivals (not to scale).

2. Far-field correlation

In order to better understand the relationship between the near-field dynamics and the far field, two-point correlations were computed (using the measured signals, as opposed to the phase-averaged waveforms) between each microphone in the near field and the far-field microphones. The correlations were then examined in the spatio-temporal domain, which showed distinct regions of positive and negative correlation spanning several jet diameters and flow time scales. The correlation regions were then compared with two expected time lags, defined similarly by other researchers[33]. The first, τ_{ac}, corresponds to the expected time lag for an acoustic wave traveling directly from the noise source to the near-field microphone and on to the far-field microphone. The second, τ_{con}, corresponds to the expected time lag for a large-scale structure to convect to the acoustic source region from the near-field microphone's axial station and radiate acoustically to the far-field microphone. A schematic of the propagation paths for the two expected time lags can be found in Figure 7. The convective velocity was assumed to be $U_c / U_j = 0.69$ (as determined by two-point correlations between neighboring near-field microphones upstream of the end of the potential core along the first microphone array position) and the acoustic source region was assumed to be $x_s/D = 4$ (this value was chosen to best match the observations made subsequently, it also corresponds to the location at which the forced jets all show significant decay in P_{ms} values). It should be noted that this analysis method is not meant to suggest that the noise generation process occurs at a specific point in space, but that the source *region* primarily exists (in a time-averaged sense) around $x/D = 4$. It should be noted that although the near-field and far-field microphone arrays are not at the same azimuthal angle with respect to the nozzle, the computations for the expected time lags do not account for this difference. It has been assumed that the acoustic radiation in jet is dominated by $m = 0$ azimuthal Fourier mode. This assumption is easily justifiable in the forced jets, where the actuators have been fired in phase. While the near-field pressure and acoustic radiation towards aft polar angles in a natural, high Reynolds number jet is a combination of numerous azimuthal Fourier modes, previous researchers

Downloaded by Mo Samimy on February 3, 2014 | http://arc.aiaa.org | DOI: 10.2514/6.2014-0527

have found these fields to be dominated by the axisymmetric Fourier mode[34-37]. Hence, the authors contend the assumption of axisymmetric noise sources and radiation is also valid in the unforced jet as well.

Results for the unforced jet can be found in Figure 8, where the space-time correlations between the near field and the far field at 30° have been plotted along two microphone array positions. To aid in identifying the physical phenomena to which the correlation regions correspond, the time lag, τ, in the figures have been non-dimensionalized by the ambient speed of sound, a_∞, and R, the distance from the near-field microphones to the far-field microphone. Close to the jet shear layer, four distinct correlation regions can be observed: two positive, two negative; one strong and one weak in each category. The first correlation regions, the strong-negative and weak-positive, are noticeable beginning at the most upstream microphone and reach their peak values around $5 < x/D < 10$, decaying significantly beyond that. The slopes of these regions indicate propagation velocities below the sonic velocity. Their slopes exhibit a gradual decay in propagation velocity; in the upstream region, they roughly match with the measured convective velocity of the large-scale structures. On the other hand, the strong-positive and weak-negative correlation regions exhibit propagation velocities that match well with the ambient speed of sound. These correlation regions start from almost negligible values upstream, strongly amplify near and just beyond the end of the potential core, and decay slightly in the most downstream region.

As the microphone array is moved radially outwards, the strong-negative and weak-positive correlation regions (associated with structure convection) quickly decay to negligible values. By $y/D = 4.20$, all observable correlation regions match the expected time-of-arrival for an acoustic wave. The distinctly different propagation velocities and axial and radial evolutions of the two pairs of correlation regions lend themselves to the hypothesis that these correspond to different physical phenomena. The strong-negative and weak-positive correlation regions observed near the jet shear layer likely are associated with the large-scale structures themselves, rather than acoustic phenomena. The positive correlation region appears to be associated with the braid region of the large-scale structure as it convects through the shear layer. The negative region corresponds to the low pressure core region of the vortex.

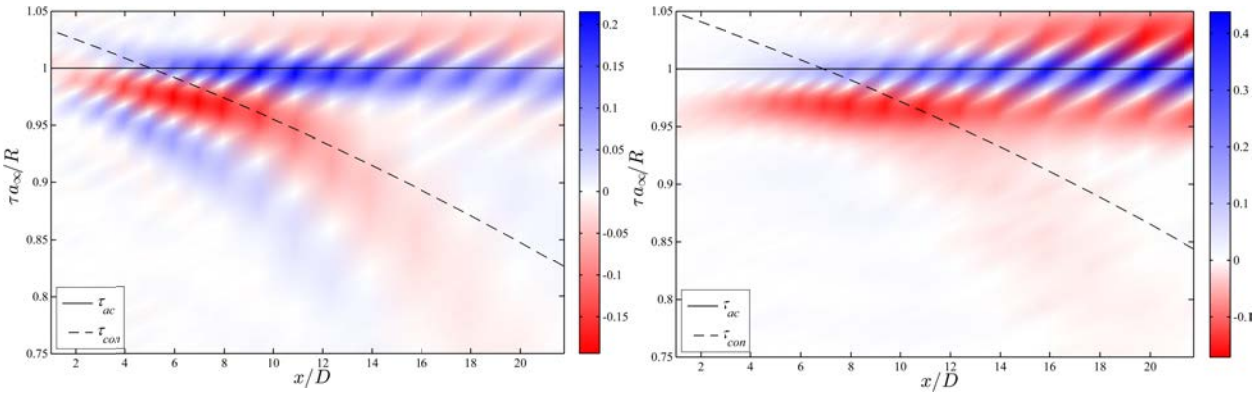

Figure 8: Normalized correlations to the far field at 30° for microphone array positions starting at y/D = 1.20 (left) and y/D = 4.20 (right) in the unforced jet.

The correlations along the first array position to the far field at 30° have been plotted in Figure 9 for the forced jets. In the case of the $St_{DF} = 0.02$ forced jet, four distinct correlation regions are observed, similar to the unforced jet. Again, the strong-positive and weak-negative correlation regions exhibit propagation velocities matching the sonic velocity in the downstream region. However, the strong-positive region no longer shows negligible correlation in the upstream region, instead exhibiting moderate correlation values and a change in slope to match the convective velocity of the large-scale structures rather than the sonic velocity. Increasing the forcing frequency to $St_{DF} = 0.15$ results in one distinct positive and negative correlation region produced per forcing period. For both positive and negative regions, the maximum correlation is found to be located $4 < x/D < 6$, which corresponds to the end of the potential core. In the upstream region, the correlations match the convective velocity and have been greatly enhanced in strength; for $x/D > \sim 8$ a marked decay is observed coinciding with a shift in propagation velocity to match the sonic velocity. In the downstream region continuously oscillation positive and negative correlation regions with sonic propagation velocities are also found, though one particular region, corresponding to the expected time-of-arrival for an acoustic wave traveling directly from the near-field microphone to the far-field microphone, is dominant over the rest. It should be noted that the positive correlation region in the upstream that merges with this particular correlation region in the downstream matches not just the convective velocity for the large-scale structures, but the expected time-of-arrival for a source that is producing acoustic radiation around the assumed

Downloaded by Mo Samimy on February 3, 2014 | http://arc.aiaa.org | DOI: 10.2514/6.2014-0527

source location, x_s/D = 4. As the forcing frequency is further increased, the region over which strong, periodic correlations with convective velocities occur decreases, from x/D < ~8 at St_{DF} = 0.15 to x/D < ~5 at St_{DF} = 0.35, as does the amplitude of the correlations. This also corresponds to a slight upstream shift in the apparent source region, as it can be seen in Figure 9c that the upstream positive correlation region which merges with the downstream correlation region occurs for time lags less than τ_{con}, suggesting the source region in this case occurs upstream of x_s/D = 4. By St_{DF} = 0.50, the correlation regions have nearly returned to the baseline state, indicating that the structures generated by the forcing at this frequency are no longer the dominant sources of noise in this jet.

The overall similarities between the correlation regions for the unforced and forced jets at a range of frequencies is highly suggestive of a consistent source mechanism (or mechanisms) for all of the jets. The trends observed in this figure are indicative of a coherent structure which convects through the shear layer in the jet core region and produces noise that radiates to the far-field just upstream of or at the end of the potential core. Similar behavior has been observed computationally[33]. The quicker decay with increasing St_{DF} of the correlation regions with convective velocities is unsurprising as it has been shown, both by previous researchers as well as by phase-averaging in this study (see Figure 3 and Figure 5), that higher frequency structures saturate and decay closer to the nozzle exit. This shift in apparent source region also matches the upstream shift in P_{ms} peak observed in Figure 5. It remains to be seen however, if the location where the dominant downstream and upstream positive correlation regions merge indicates the beginning of the source region, or if acoustic radiation from the large-scale structures exists in the most upstream region and it is being masked by the correlations to the large-scale structures. It is this question that the subsequent sections strive to answer.

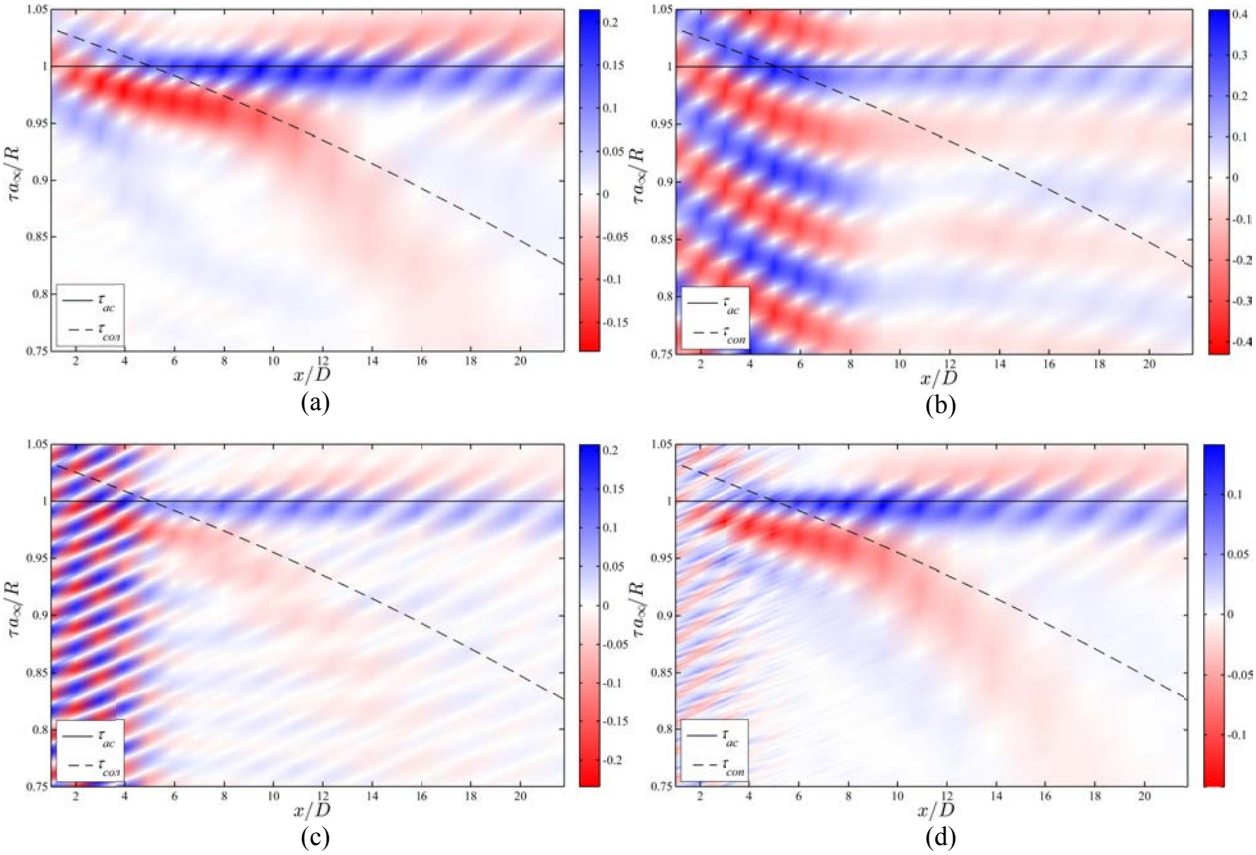

Figure 9: Normalized correlation along the first array position to the far field at 30° for St_{DF} = 0.02 (a), St_{DF} = 0.15 (b), St_{DF} = 0.35 (c), and St_{DF} = 0.50 (d).

B. Wavenumber-frequency filtering

The results of the wavenumber-frequency filtering in the unforced jet can be seen in Figure 10, where the power spectral densities for the total, hydrodynamic, and acoustic waveforms in the unforced jet have been plotted along the first microphone array position at x/D = 6 and x/D = 11. Three vertical lines have been overlain: dash, dash-dot, and dotted. These correspond to the critical frequency, and the far-field spectral peak at 30° and 90°, respectively. The critical frequency, the frequency near which the near-field spectra transition from hydrodynamically dominated

Downloaded by Mo Samimy on February 3, 2014 | http://arc.aiaa.org | DOI: 10.2514/6.2014-0527

to acoustically dominated (as evident from the change of spectral slope), has been shown[21] to scale as fy/U_c, resulting in a consistent value of unity. As before, the convective velocity is assumed to be $0.69U_j$. As expected, the hydrodynamic component matches well with the total signal in the low frequency portions of the spectra, while the acoustic component matches well in the high frequency portions. At both axial locations, the critical frequency reasonably predicts the cross-over in amplitude between the hydrodynamic and acoustic components. This can also be observed in Figure 11, where the decomposed spectra at $x/D = 6$ has been plotted for the array position starting at $y/D = 4.20$. As before, the critical frequency continues to predict well the cross-over frequency for the two components.

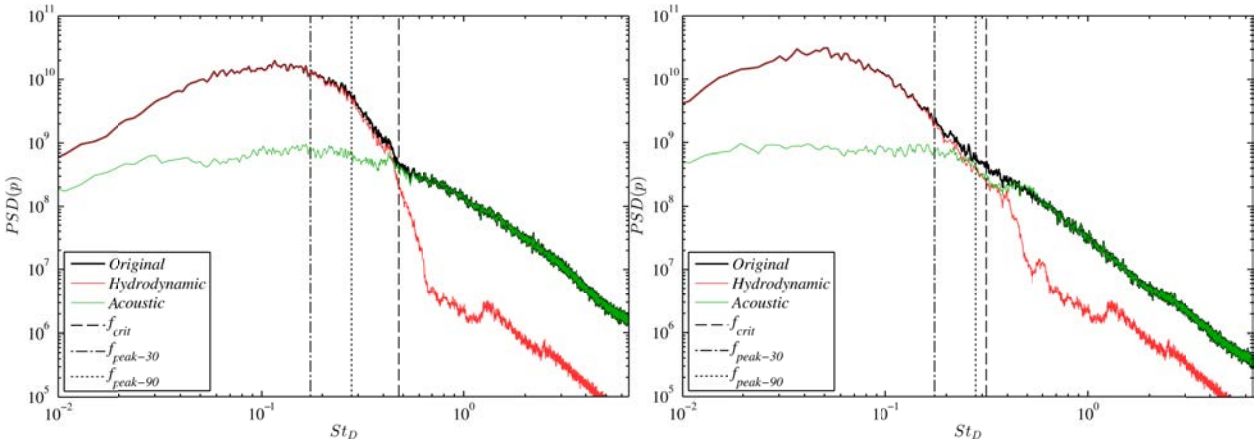

Figure 10: Decomposed spectra for unforced jet along first array position at $x/D = 6$ (left) and $x/D = 11$ (right). Dashed vertical line denotes the critical frequency, $fy/U_c = 1$.

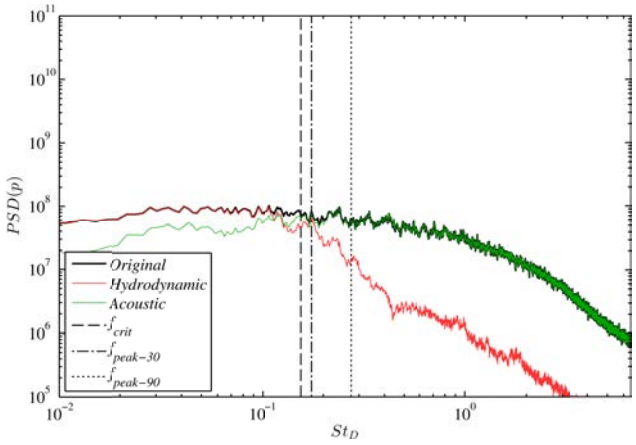

Figure 11: Decomposed spectra along seventh array position ($y/D = 4.20$) at $x/D = 6$, for the unforced jet.

A change in shape in the acoustic spectra is evident with axial and radial distance: at locations corresponding to low angles with respect to the jet axis (Figure 10), the spectrum is more 'peaky' (reminiscent of far-field spectra at aft angles) and the acoustic peak frequency matches well with the far-field peak at 30°. At locations corresponding to high angles (Figure 11) the acoustic spectrum is more broadband and rounded (reminiscent of the well-known shape of the far-field spectra at sideline angles[2] – this is especially apparent at the farther array positions) and the acoustic peak frequency matches well with the far-field peak at 90°. It should be noted that previous researchers have identified the end of the potential core as a dominant noise source region in subsonic jets[38].

Results for the decomposed waveforms at $x/D = 11$ along the first microphone array position are shown in Figure 12 for select forcing frequencies. As before, the critical frequency for this microphone position has been denoted by a dashed vertical line. Additionally, the first five forcing tones in the far-field spectra at 30° are indicated by black markers at the top of the plots. Though not shown here for brevity, similar trends to the unforced jet results are found, in terms of cross-over frequency between the hydrodynamic and acoustic components and change in acoustic spectral shape and peak frequency with position. The spectra for the hydrodynamic and acoustic fields both consistently show sharp tones at the fundamental forcing frequency as well as its higher harmonics, regardless of the

Downloaded by Mo Samimy on February 3, 2014 | http://arc.aiaa.org | DOI: 10.2514/6.2014-0527

position of the microphone. Of special interest are the results for St_{DF} = 0.05 (Figure 12a); though the original spectra contain only the fundamental forcing tone, the acoustic spectra contain the fundamental as well as five harmonic tones, matching what is observed at the far-field aft angle. While it is surprising that the tonal amplitude exceeds that of the total waveform, an effect which can be produced by the application of the window function and Gaussian cut-off, it is unlikely that the wavenumber-filtering is producing completely spurious tones. Several different widths for the Gaussian cut-off, including a sharp cut-off, were evaluated, along with using a Hamming window in place of the Tukey window, all of which resulted in acoustic spectra displaying tonal energy at the fundamental and harmonics of the forcing frequency (though at different amplitudes). A more in-depth parametric study of these effects is currently underway. Overall however, the results found in Figure 12 lend strong credence to the argument that the wavenumber-frequency filtering is producing a realistic reconstruction of the hydrodynamic and acoustic fields in both the forced and unforced jets, and accurately capturing the dynamics of the large-scale structures and their radiated noise.

Owing to the discrete nature of the Fourier transform being performed, some energy leakage between the acoustic and hydrodynamic components is unavoidable. The effects of this leakage are most apparent in the hydrodynamic spectra at high frequencies and the acoustic spectra at low frequencies. In both cases, the leakage is producing non-physical decay rates in the spectra; this may be overcome in the future by appropriate bandpass filtering in post-processing. Nonetheless, the results shown here are quite promising.

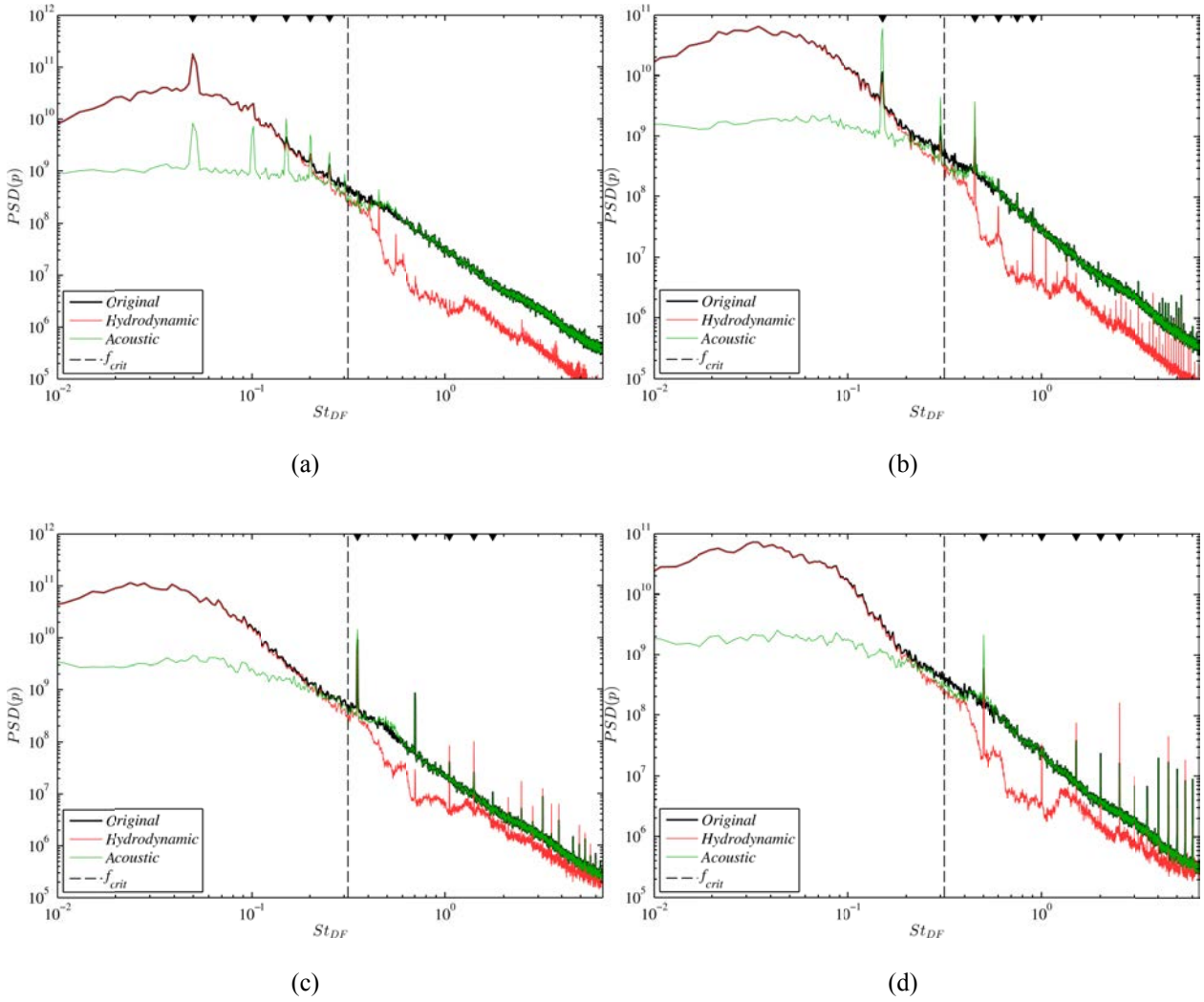

Figure 12: Decomposed spectra for forced jet along first array position at x/D = 11; dashed vertical line denotes the critical frequency, fy/U_c = 1, markers correspond to first five spectral tones in the far-field at 30°. Forcing frequencies correspond to St_{DF} = 0.05 (a), St_{DF} = 0.15 (b), St_{DF} = 0.35 (c), and St_{DF} = 0.50 (d).

Downloaded by Mo Samimy on February 3, 2014 | http://arc.aiaa.org | DOI: 10.2514/6.2014-0527

Downloaded by Mo Samimy on February 3, 2014 | http://arc.aiaa.org | DOI: 10.2514/6.2014-0527

C. Response of the decomposed fields

Subsequent to the wavenumber-frequency filtering, the decomposed fields were phase-averaged akin to the results shown in §III.A. Results for $St_{DF} = 0.05$ are shown in Figure 13, where the original and decomposed phase-averaged waveforms have been plotted for two axial positions, $x/D = 3$ and $x/D = 11$, along the first array position. In this case, the waveforms have been plotted for one complete forcing period. In both cases the hydrodynamic waveform closely matches the original waveform, which is unsurprising given the proximity of the microphone array to the jet shear layer. What is interesting though, is the existence of distinct acoustic fluctuations at all axial positions observed, which have a characteristic shape that is fundamentally different from the original and hydrodynamic waveforms. (The discrete Fourier transform inherent in the wavenumber-frequency filtering necessitates application of a window function to the raw waveforms prior to the forward transform – an unfortunate effect of this is the corruption of the reconstructed waveforms near the spatial boundaries, hence these locations are not included in the following analysis.)

In the upstream position, the acoustic waveform exhibits multiple compression and expansion waves and is of much lower amplitude than the hydrodynamic. Here, both the waveforms represent an impulse response in which the jet returns to its natural state before the next forcing period. In the downstream location, the acoustic waveform has evolved to one in which a dominant expansion wave is trailed by a dominant compression wave. More importantly, the acoustic waveform again represents an impulse response, whereas the hydrodynamic field exhibits a periodic fluctuation of interacting large-scale structures. This compares well with the waveform found at the far-field aft angles (Figure 6) at this St_{DF}, which also exhibited an impulse response consisting of an expansion wave trailed by a compression wave.

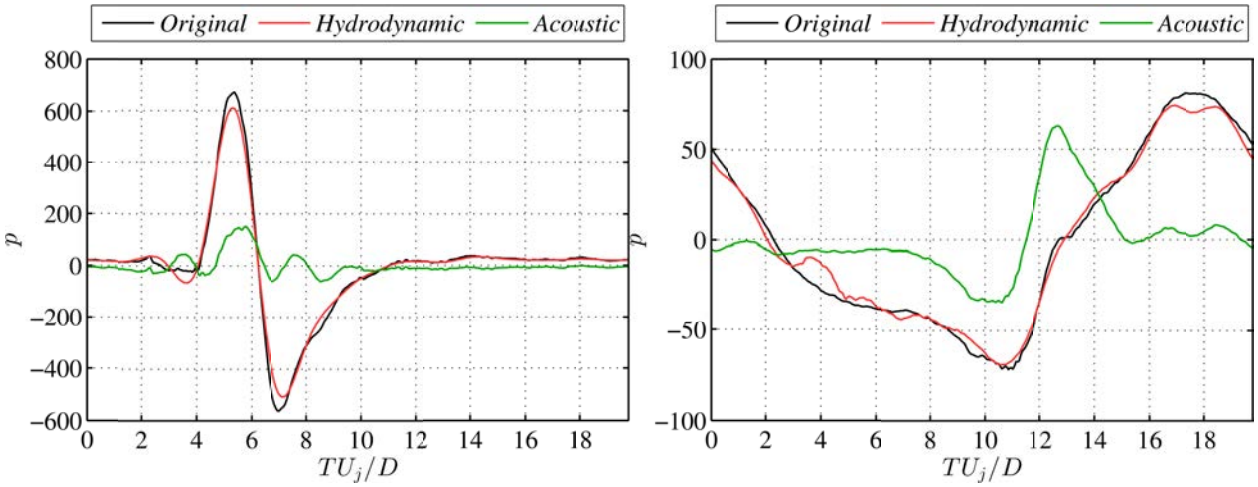

Figure 13: Phase-averaged waveforms of the decomposed fields for $St_{DF} = 0.05$ along the first microphone array position at $x/D = 3$ (left) and $x/D = 11$ (right).

Similarly, the results at higher St_{DF}, a sample of which can be found in Figure 14, show coherent radiation over the entire domain explored in this study (again, excluding the corrupted boundaries). Due to the reduced forcing period, the response of the acoustic field is now periodic rather than impulsive. In the case of moderate forcing frequencies for which the generated structures are just beginning to linearly interact ($St_{DF} = 0.15$), the shape of the impulse acoustic response seen for $St_{DF} = 0.05$ is more or less retained, with one primary compression wave leading (or followed) by two smaller waves. Further increases in the forcing frequency to $St_{DF} = 0.35$ result in significant alteration to the shape of the acoustic response. However, it can be shown that the waveform shape (if not the peak amplitude) can be well predicted by a linear superposition of the fundamental acoustic response, as in §III.A. In Figure 15 the fundamental acoustic response to forcing ($St_{DF} = 0.05$) and the periodic response ($St_{DF} = 0.35$) has been plotted for $x/D = 3$. Additionally, a linear superposition of the fundamental response repeated at the periodic frequency has been included. It is found that the linear superposition of the fundamental response matches the periodic response in shape and overall amplitude quite well, the only significant discrepancies being the peak amplitude of the of the compression and expansion waves. This strong similarity in the acoustic response to a broad range of forcing frequencies spanning the impulsive and periodic regimes indicates a consistent dominant source mechanism for the large-scale structures.

Currently the cause of the discrepancy in peak amplitude is unknown, though it may be due to nonlinear effects. While the evolution of the large-scale structures produced by forcing at $St_{DF} = 0.35$ can largely be described by the

aforementioned linear superposition model, the scale and amplitude of the structures makes it likely that nonlinearities play a non-negligible role, one that has been observed in linear and nonlinear stability theory. Indeed, Sinha et al.[21] argued that this was the case for the jet forced near the jet column mode (roughly St_{DF} = 0.35 for this jet). Whatever the cause, the structures in the forced jet undergo significant amplitude modulation in the upstream region (particularly for St_{DF} = 0.15 to 0.35), as can be observed in the P_{ms} fluctuations (Figure 5). Using a Gaussian wavepacket source model, Cavalieri et al.[39] showed that spatial (as well as temporal) modulation of the source resulted in an increase of the peak amplitude of the acoustic response. Similar dynamics may be at work here.

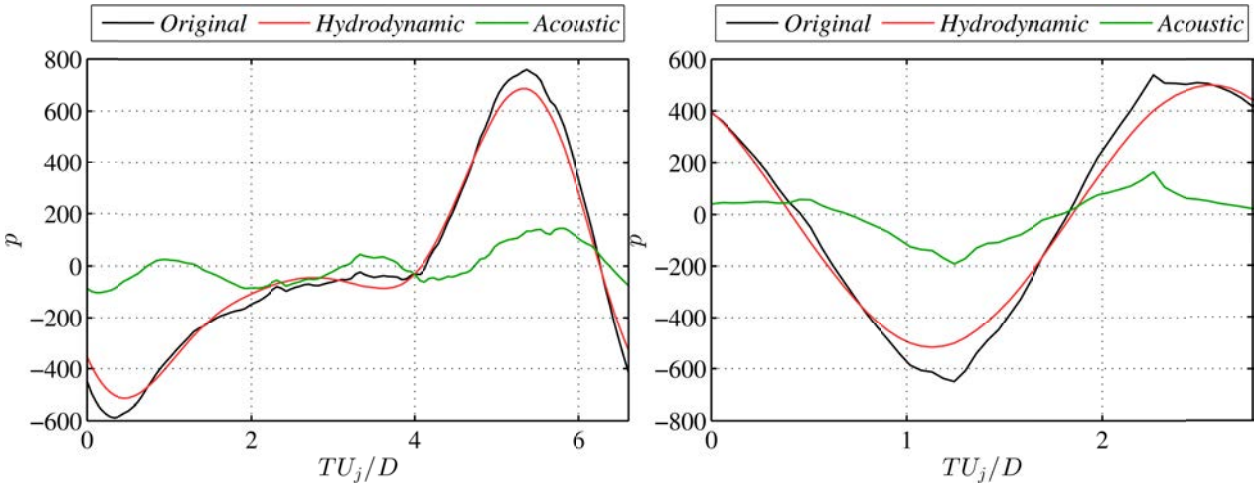

Figure 14: Phase-averaged waveforms of the decomposed fields for St_{DF} = 0.15 (left) and St_{DF} = 0.35 (right) along the first microphone array position at x/D = 3.

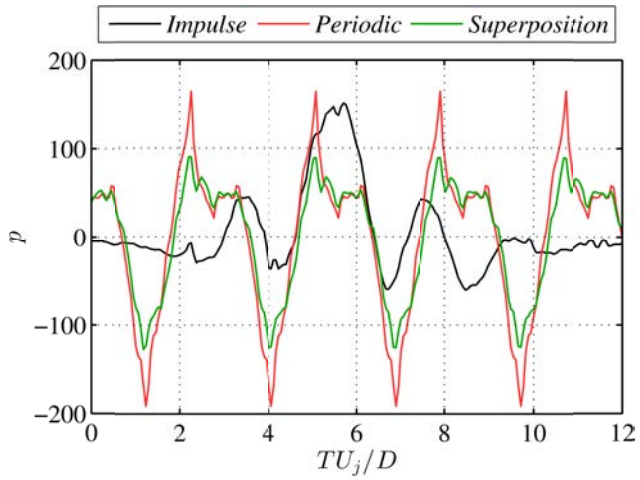

Figure 15: Effect of periodicity of the forcing on the acoustic response of the jet at x/D = 3 in which the periodic response at St_{DF} = 0.35 is modeled as a linear superposition of the impulse response repeated at the periodic frequency.

Experimental as well as theoretical results have shown that the acoustic sources in subsonic, unheated jets exhibit a quadrupole-like radiation pattern to the far field, with the primary radiation angle directed towards the aft angles and the amplitude decaying exponentially with increasing polar angle. Nonetheless, acoustic propagation is spherical, centered on the source region, and hence acoustic waves observed in the upstream region may in fact have their source in the downstream region. In order to investigated the source location for these upstream acoustic waves (in an approximate sense), two-point correlations between the near field and far field at 30° were recomputed using only the acoustic component in the near field. As before, the two expected time lags, τ_{ac} and τ_{con}, have been overlain on the plots, and the abscissa has been normalized at each axial position by the ambient speed of sound and the distance from the near-field microphone to the far-field microphone. As with the phase-averaged waveforms for the decomposed fields, the correlations in the most upstream and downstream regions have been omitted due to boundary effects from the windowing and DFT.

Downloaded by Mo Samimy on February 3, 2014 | http://arc.aiaa.org | DOI: 10.2514/6.2014-0527

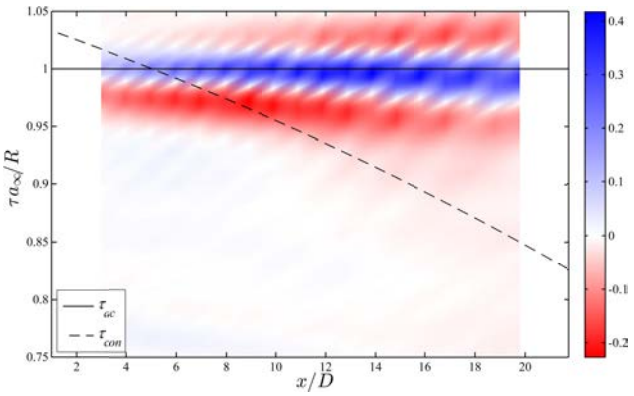

Figure 16: Normalized correlations of the acoustic near-field response in the unforced jet to the far field at 30° for the first microphone array position, starting at *y/D* = 1.20.

Results shown in Figure 16 correspond to the unforced jet along the first array position. A marked change in the upstream region is apparent when comparing these results against those for the full near field (Figure 8). No correlation regions matching the convectively velocity of the large-scale structures exist; this confirms our previous assertion that the upstream correlation regions in Figure 8 were associated with the large-scale structures themselves, rather than direct acoustic phenomena. Instead a single positive correlation region, roughly matching τ_{ac}, exists over the entire domain with significantly enhanced correlation over the full field results. In fact, the results found here for the acoustic component along the first microphone array position are nearly identical to those for the full field response at the further array positions (Figure 8).

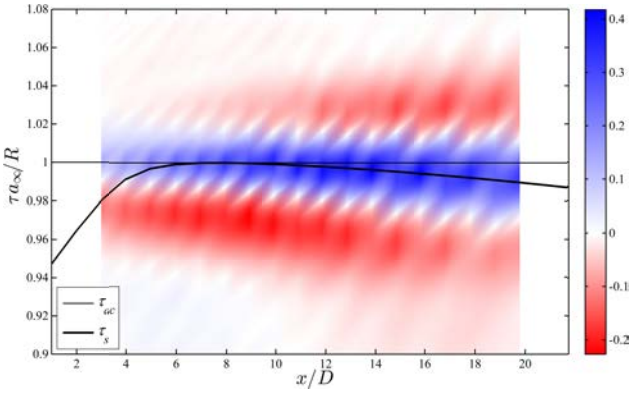

Figure 17: Normalized correlations in the unforced jet to the far field at 30°, with time lags indicating a moving and stationary (in space) source region.

Though initially overlooked, upon closer inspection it becomes apparent that the positive correlation region does not line up exactly with τ_{ac}, the mismatch becoming progressively greater with downstream distance. This behavior can be seen more clearly in Figure 17, in which the previous results have been replotted over a shorter period of time. As the near-field probes are located outside the source region, calculation of an expected time-of-arrival for an acoustic wave requires an assumption about the location of the source region. In formulating τ_{ac}, it was assumed that the source region lay directly on the line connecting the near-field microphone to the far-field microphone. Another expected time-of-arrival can be constructed by assuming the source region is stationary in space; from simple geometric considerations of the distance from the assumed source region to the near-field and far-field microphones, the time lag, τ_s, between the arrival of an acoustic wave at both microphones can be computed. For the unforced jet, the acoustic source was assumed to be located at $x_s/D = 4$ (as before, this type of analysis is not meant to imply that the source region is located at a specific, fixed point – it is merely a convenient way of understanding the propagation paths). In the upstream region of the jet, the peaks of the positive correlation region match τ_{ac} nearly exactly. In the downstream region, τ_{ac} begins to increasingly over-predict the time lag for the maximum correlation. On the other hand, τ_s tracks the time lags for the peak correlation consistently over the downstream region, but not the upstream region. The results found here indicate that the dominant acoustic radiation reaching the far-field aft angles is being generated over an extended region of the jet mixing layer, roughly $x/D \leq 4$ in the case of the unforced jet.

Downloaded by Mo Samimy on February 3, 2014 | http://arc.aiaa.org | DOI: 10.2514/6.2014-0527

Similar calculations were carried out for the forced jets, and the results are shown in Figure 18. For very low St_{DF}, for which the structures evolve independently before passing through the end of the potential core (Figure 18a), the correlation regions are nearly unchanged from the unforced jet. As before, the upstream peak correlations match with τ_{ac} while the downstream match with τ_s with x_s set to $4D$, again indicating that the acoustic fluctuations measured in the downstream are predominantly being generated upstream, before the end of the potential core. As the forcing frequency is increased and the generated structures begin undergoing significant linear interactions as they advect through the mixing layer upstream of the end of the potential core (Figure 18b & c), the assumed source region, x_s, must be shifted upstream to $1D$ for τ_s to continue to match with the peak correlation values in the downstream. This upstream shift is unsurprising, given that it has already been shown that the higher frequency structures saturate and begin to decay further upstream than the lower frequency structures. By $St_{DF} = 0.50$ however, the correlation regions have returned to their unforced state – possibly reinforcing the previous hypothesis that the structures generated by this forcing no longer constitute the dominant source in this jet.

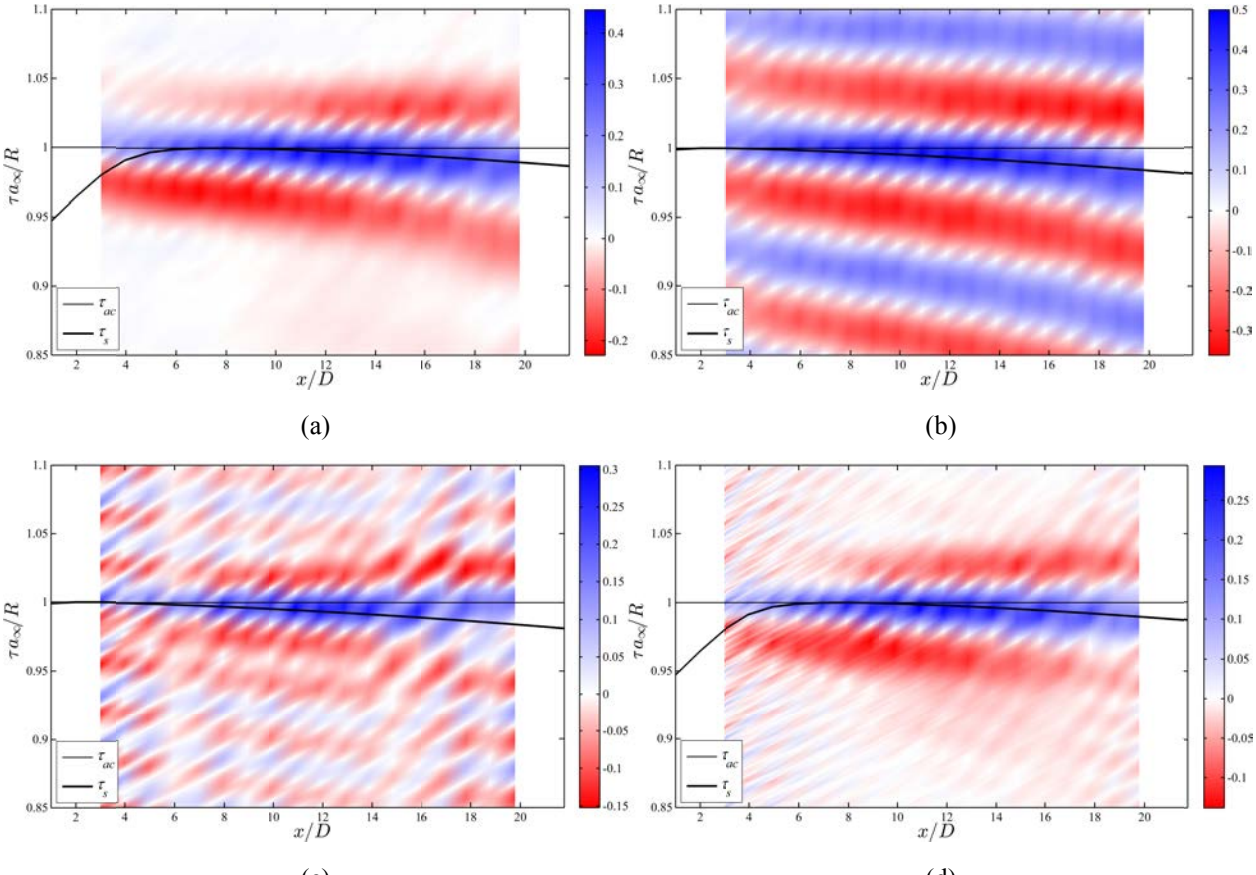

Figure 18: Normalized correlations of the acoustic near-field response along the first array position to the far field at 30° in the forced jet at $St_{DF} = 0.05$ (a), $St_{DF} = 0.15$ (b), $St_{DF} = 0.35$ (c) and $St_{DF} = 0.50$ (d). The assumed source location was not held constant for the different forcing conditions, being set to $4D$, $1D$, $1D$, and $4D$, respectively.

D. Coherence of the response

Up to this point, our analysis has relied on some sort of temporal-averaging: either the phase-averaging, the sliding convolution inherent in two-point correlations or even the time-integral necessary for computation of the power spectral density. This reduction in complexity greatly simplifies our analysis of the turbulent jet, though it comes at a significant cost in terms of the information lost. As other researchers have shown[9,40], subsonic jet noise is a highly intermittent phenomena, the fine details of which may be smeared or completely masked by this temporal-averaging. Wavelet analysis, in which a user-defined mother wavelet is used as the basis function, has been used by numerous researchers to investigate the time-domain behavior of temporally-localized phenomena. By using a basis, which is localized in both time and space, wavelet analysis overcomes many of the drawbacks of the Fourier-based

Downloaded by Mo Samimy on February 3, 2014 | http://arc.aiaa.org | DOI: 10.2514/6.2014-0527

spectrogram method (sliding Fourier transform). An excellent overview of wavelet data analysis may be found in Torrence & Campo[41], from which the wavelet software used in this study was adopted. In this work, preliminary investigation into the time-domain behavior of the hydrodynamic and acoustic response of the jet to forcing is accomplished using the Paul and Morlet wavelet bases, respectively. These mother wavelets were chosen as they best matched the shape of the phase-averaged, fundamental responses in the hydrodynamic and acoustic fields, respectively; other wavelet bases were found to produce qualitatively similar results, though due to the mismatch in response and basis shape, individual events in the time traces were either smeared or appeared as multiple events.

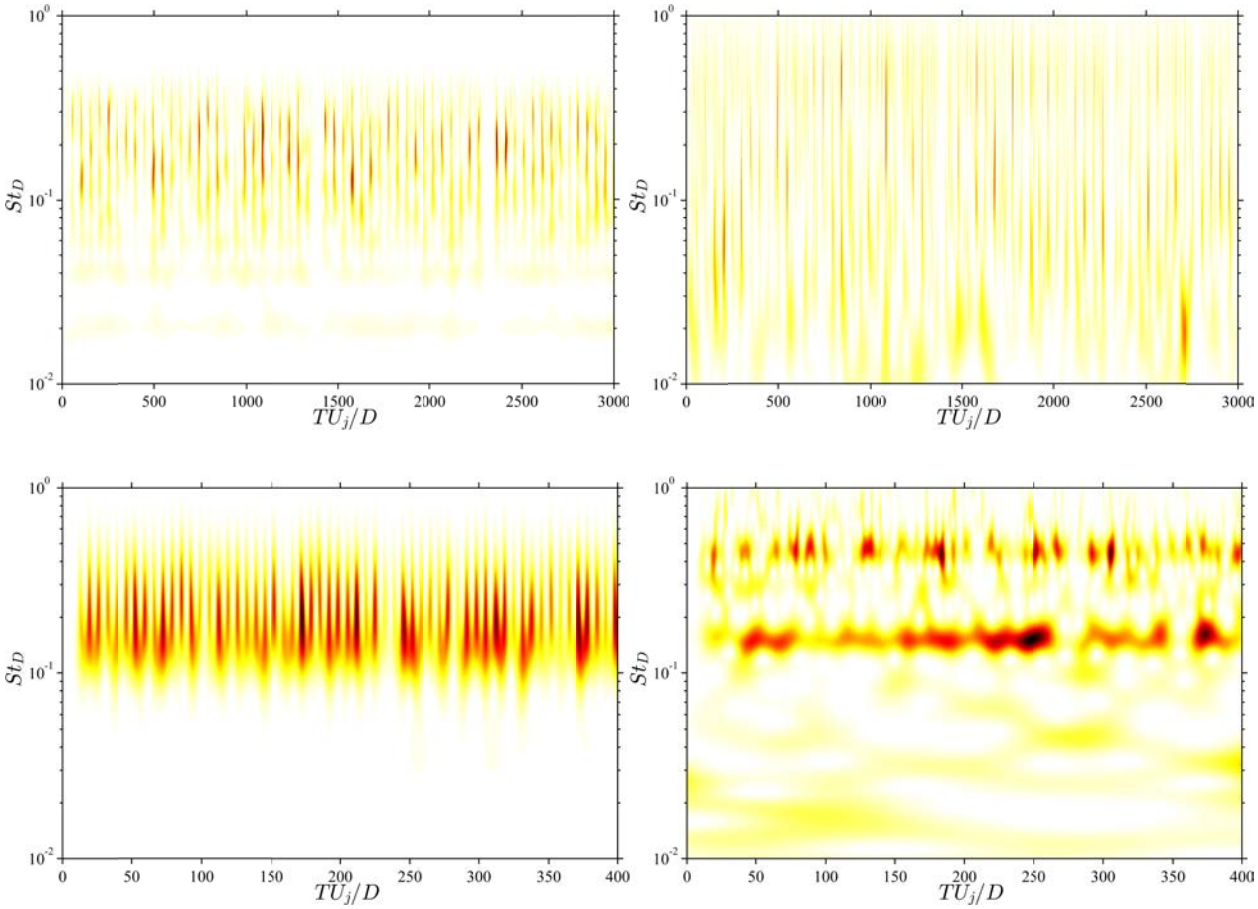

Figure 19: Wavelet coefficient energies for hydrodynamic (left column) and acoustic (right column) components for St_{DF} = 0.02 (top row) and St_{DF} = 0.15 (bottom row) at x/D = 3. Wavelet coefficients have been normalized to have energy of unity at all scales, and wavelet scales have been converted to pseudo-frequency.

Results for two forcing cases, St_{DF} = 0.02 and St_{DF} = 0.15, have been included in Figure 19, in which the wavelet power spectra has been plotted for the hydrodynamic and acoustic components at an axial station of x/D = 3. The reader is reminded that at this location, the structures generated at St_{DF} = 0.02 are evolving independently while those at St_{DF} = 0.15 are beginning to linearly interact (refer to Figure 3). Note that the abscissa is not consistent between the two forcing frequencies; the results at the lower frequency have been plotted over a proportionally longer time scale so that an equal number of forcing periods are shown for the two frequencies. Comparing the hydrodynamic fields, similar results are found for the impulse- and period-forced jets. Though there is some variability in the response of the jet to the forcing (particularly at the lower frequency), in both cases repeatable, coherent structures are observed at the forcing frequency with a well-defined and relatively consistent energy content. This is not the case for the acoustic field, however. In the higher frequency case, in which the structures generated by forcing are linearly interacting, consistent energy bands at the forcing frequency and its second harmonic are observed. Though the events in the acoustic field are less consistent than those in the hydrodynamic, they still represent a semi-coherent response to the forcing. In contrast, the acoustic response to impulse forcing shows no discernible energy bands or repeatable events at the forcing frequency (the results shown here are

Downloaded by Mo Samimy on February 3, 2014 | http://arc.aiaa.org | DOI: 10.2514/6.2014-0527

qualitatively similar to those for the unforced jet). The coherent interactions produced by the periodic forcing are themselves producing, either directly or indirectly, relatively coherent acoustic radiation. The incoherent interactions in the impulse forced jet (the structures generated by forcing are of course interacting with the incoherent background turbulence) are producing incoherent radiation.

This result may seem to contradict those shown previously, in which phase-averaging of the acoustic field showed a coherent response to the impulse forcing. It is improbable that the phase-averaged acoustic response to periodic forcing could be constructed as a superposition of impulse responses if the impulse response itself did not actually correspond to anything physical. Surely, this 'fundamental' response is not merely a false artifact of the averaging process. Likely, this phase-averaged response to impulse forcing represents the average response of the large-scale structure generated by the forcing to the interactions with structures over the entire range of (noise producing) scales present in the turbulent jet.

IV. Conclusions

The actuators used in this study provide a unique opportunity to investigate the dynamics of large-scale structures, the noise sources, and the radiated noise; the well-defined actuation phase enables phase-averaging of the pressure signal. Hence, time-resolved (more precisely phase-resolved) measurements over an entire region of the near-field may be acquired and correlated, providing additional insight into the noise sources than the conventional two-point correlations.

Results showed that the forcing produces coherent, large-scale structures which grow, interact, decay, and generate radiation to the far field. When forcing at very low frequencies (impulse forcing), the structures evolve independently (from the other structures generated by forcing, though not the baseline turbulence) as they advect through the shear layer, representing the fundamental response of the jet to a perturbation. As the forcing frequency is raised, the generated structures begin to interact before passing through the end of the potential core. It was found that the waveform amplitude and shape in this forcing regime ($0.15 \leq St_{DF} \leq 0.50$) could be well predicted by a linear superposition of the fundamental response of the jet, indicating that the structure dynamics were predominantly linear in nature. Two-point correlations between the near field and the far field at aft angles showed correlation regions matching the characteristics of convecting large-scale structures in the upstream measurement domain and pure acoustic radiation in the downstream. Aside from slight upstream shift in the apparent source region, the correlations showed little characteristic changes over the range of Strouhal numbers explored in this study, suggesting a consistent dominant source mechanism for the noise generation process between the independently and linearly-interacting structure evolution.

By applying a digital filter to the near-field measurements along each microphone array position, the near-field pressure can be decomposed into its constitutive hydrodynamic and acoustic components based on the phase velocity for each frequency-wavenumber pair. Examination of the spectra for the individual components revealed cross-over between the spectral amplitudes at the critical frequency identified by previous researchers, as well as changes in the acoustic spectra in relation to the end of the potential core that match the previously observed features of the far-field spectra. Subsequent phase-averaging of the decomposed acoustic near-field, as well as two point correlations with the far field found that the forcing resulted in acoustic waves which had their origins in the upstream portion of the jet, before the end of the potential core. The apparent source region was observed to shift upstream with higher frequencies, in agreement with past results. As with the structures themselves, the acoustic response to periodic forcing could be well modeled as a linear superposition of the fundamental response; this strongly suggests a consistent source mechanism over the range of large-scale structures encountered in this study.

Though phase-averaging and two-point correlations remain useful analysis tools for simplifying and understanding the dynamics of the turbulent jet, the temporal-averaging inherent in these techniques masks important features of the response of the jet. Preliminary investigation of the temporal coherency of the response of jet by way of wavelet analysis found highly intermittent acoustic events, over a broad range of scales, when the jet is forced in the impulse regime. Increasing the forcing frequency such that the structures began linearly interacting resulted in a regularization of the acoustic response. Further investigation into the intermittency of the acoustic response is clearly warranted.

Acknowledgements

The support of this work by the Air Force Office of Scientific Research (Dr. John Schmisseur and Dr. Rengasamy Ponnappan) is appreciated.

Downloaded by Mo Samimy on February 3, 2014 | http://arc.aiaa.org | DOI: 10.2514/6.2014-0527

References

[1]Lighthill, M. J. "On Sound Generated Aerodynamically. I. General Theory," *Proceedings of the Royal Society of London: Series A, Mathematical and Physical Sciences*. Vol. 211, The Royal Society, 1952, pp. 564-587.

[2]Tam, C. K. W., Viswanathan, K., Ahuja, K., and Panda, J., "The Source of Jet Noise: Experimental Evidence," *Journal of Fluid Mechanics*, Vol. 615, 2008, pp. 253-292.

[3]Mollo-Christensen, E., "Jet Noise and Shear Flow Instability Seen From an Experimenter's Viewpoint," *ASME Journal of Applied Mechanics*, Vol. 34, 1967, pp. 1-7.

[4]Crow, S. C., and Champagne, F. H., "Orderly Structure in Jet Turbulences," *Journal of Fluid Mechanics*, Vol. 48, No. 3, 1971, pp. 547-591.

[5]Moore, C. J., "The role of shear-layer instability waves in jet exhaust noise," *Journal of Fluid Mechanics*, Vol. 80, No. 2, 1977, pp. 321-367.

[6]Jordan, P., and Colonius, T., "Wave Packets and Turbulent Jet Noise," *Annual Review of Fluid Mechanics*, Vol. 45, 2013, pp. 173-195.

[7]Crighton, D. G., and Huerre, P., "Shear-layer pressure fluctuations and superdirective acoustic sources," *Journal of Fluid Mechanics*, Vol. 220, 1990, pp. 355-368.

[8]Sandham, N. D., Morfey, C. L., and Hu, Z. W., "Nonlinear mechanisms of sound generation in a perturbed parallel jet flow," *Journal of Fluid Mechanics*, Vol. 565, 2006, pp. 1-23.

[9]Cavalieri, A. V. G., Jordan, P., Gervais, Y., Wei, M., and Freund, J. B., "Intermittent sound generation and its control in a free-shear flow," *Physics of Fluids*, Vol. 22, 2010, p. 115113.

[10]Samimy, M., Adamovich, I., Webb, B., Kastner, J., Hileman, J., Keshav, S., and Palm, P., "Development and characterization of plasma actuators for high-speed jet control," *Experiments in Fluids*, Vol. 37, No. 4, 2004, pp. 577-588.

[11]Utkin, Y. G., Keshav, S., Kim, J.-H., Kastner, J., Adamovich, I. V., and Samimy, M., "Development and use of localized arc filament plasma actuators for high-speed flow control," *Journal of Physics D: Applied Physics*, Vol. 40, No. 3, 2007, pp. 685-694.

[12]Samimy, M., Kim, J. H., Kastner, J., Adamovich, I., and Utkin, Y., "Active Control of a Mach 0.9 Jet for Noise Mitigation Using Plasma Actuators," *AIAA Journal*, Vol. 45, No. 4, 2007, pp. 890-901.

[13]Kim, J. H., Kastner, J., and Samimy, M., "Active Control of a High Reynolds Number Mach 0.9 Axisymmetric Jet," *AIAA Journal*, Vol. 47, No. 1, 2009, pp. 116-128.

[14]Samimy, M., Kim, J. H., Kastner, J., Adamovich, I., and Utkin, Y., "Active Control of High-Speed and High-Reynolds-Number Jets Using Plasma Actuators," *Journal of Fluid Mechanics*, Vol. 578, No. 1, 2007, pp. 305-330.

[15]Kim, J.-H., and Samimy, M., "Effects of Active Control on the Flow Structure in a High Reynolds Number Supersonic Jet," *International Journal of Flow Control*, Vol. 1, No. 2, 2009, pp. 99-117.

[16]Samimy, M., Kim, J.-H., Kearney-Fischer, M., and Sinha, A., "Acoustic and flow fields of an excited high Reynolds number axisymmetric supersonic jet," *Journal of Fluid Mechanics*, Vol. 656, 2010, pp. 507-529.

[17]Kim, J.-H., Kearney-Fischer, M., Samimy, M., and Gogineni, S., "Far-field Noise Control in Supersonic Jets Using Conical and Contoured Nozzles," *ASME Journal of Engineering for Gas Turbine and Power*, Vol. 133, 2011, p. 081201.

[18]Kearney-Fischer, M., Kim, J.-H., and Samimy, M., "Noise Control of a High Reynolds Number High Speed Heated Jet Using Plasma Actuators," *International Journal of Aeroacoustics*, Vol. 10, No. 5-6, 2011, pp. 635 – 658.

[19]Samimy, M., Kearney-Fischer, M., Kim, J.-H., and Sinha, A., "High-Speed and High-Reynolds-Number Jet Control Using Localized Arc Filament Plasma Actuators," *Journal of Propulsion and Power*, Vol. 28, No. 2, 2012, pp. 269-280.

[20]Kearney-Fischer, M., Kim, J.-H., and Samimy, M., "A Study of Mach Wave Radiation Using Active Control," *Journal of Fluid Mechanics*, Vol. 681, 2011, pp. 261-292.

[21]Sinha, A., Alkandry, H., Kearney-Fischer, M., Samimy, M., and Colonius, T., "The impulse response of a high-speed jet forced with localized arc filament plasma actuators," *Physics of Fluids*, Vol. 24, 2012, p. 125104.

[22]Alkandry, H., Crawley, M., Sinha, A., Kearney-Fischer, M., and Samimy, M., "An Investigation of the Irrotational Near Field of an Excited High-Speed Jet," *51st AIAA Aerospace Sciences Meeting*, AIAA 2013-0325, 2013.

[23]Crawley, M., Alkandry, H., Sinha, A., and Samimy, M., "Correlation of Irrotational Near-Field Pressure and Far-Field Acoustic in Forced High-Speed Jets," *19th AIAA/CEAS Aeroacoustics Conference*, 2013-2188, 2013.

[24]Tinney, C. E., and Jordan, P., "The near pressure field of co-axial subsonic jets," *Journal of Fluid Mechanics*, Vol. 611, 2008, pp. 175-204.

Downloaded by Mo Samimy on February 3, 2014 | http://arc.aiaa.org | DOI: 10.2514/6.2014-0527

[25]Hahn, C., "Design and Validation of the New Jet Facility and Anechoic Chamber," M.S. Thesis, Mechanical Engineering, The Ohio State University, Columbus, OH, 2011.
[26]Kearney-Fischer, M., Kim, J.-H., and Samimy, M., "Control of a high Reynolds number Mach 0.9 heated jet using plasma actuators," *Physics of Fluids*, Vol. 21, 2009, p. 095101.
[27]Hahn, C., Kearney-Fischer, M., and Samimy, M., "On factors influencing arc filament plasma actuator performance in control of high speed jets," *Experiments in Fluids*, Vol. 51, No. 6, 2011, pp. 1591-1603.
[28]Coiffet, F., Jordan, P., Delville, J., Gervais, Y., and Ricaud, F., "Coherent structures in subsonic jets: a quasi-irrotational source mechanism?," *International Journal of Aeroacoustics*, Vol. 5, No. 1, 2006, pp. 67 - 89.
[29]Guitton, A., Kerherve, F., Jordan, P., and Delville, J., "The sound production mechanism associated with coherent structures in subsonic jets," *AIAA/CEAS 14th Aeroacoustics Conference*, 2008-2892, 2008.
[30]Hussain, A. K. M. F., and Reynolds, W. C., "The mechanics of an organized wave in turbulent shear flow," *Journal of Fluid Mechanics*, Vol. 41, 1970, pp. 241-258.
[31]Suzuki, T., and Colonius, T., "Instability waves in a subsonic round jet detected using a near-field phased microphone array," *Journal of Fluid Mechanics*, Vol. 565, 2006, pp. 197-226.
[32]Ukeiley, L. S., and Ponton, M. K., "On the near field pressure of a transonic axisymmetric jet," *International Journal of Aeroacoustics*, Vol. 3, No. 1, 2004, pp. 43-66.
[33]Bogey, C., and Bailly, C., "An analysis of the correlations between the turbulent flow and the sound pressure fields of subsonic jets," *Journal of Fluid Mechanics*, Vol. 583, 2007, pp. 71-97.
[34]Arndt, R. E. A., Long, D. F., and Glauser, M. N., "The proper orthogonal decomposition of pressure fluctuations surrounding a turbulent jet," *Journal of Fluid Mechanics*, Vol. 340, 1997, pp. 1-33.
[35]Hall, J. W., Pinier, J., Hall, A. e., and Glauser, M., "Two-point correlations of the near and far-field pressure in a transonic jet," *ASME 2006 Joint U.S. European Fluids Engineering Summer Meeting*, FEDSM2006-98458, 2006.
[36]Kœnig, M., Cavalieri, A. V. G., Jordan, P., and Gervais, Y., "Intermittency of the azimuthal components of the sound radiated by subsonic jets," *AIAA/CEAS 17th Aeroacoustics Conference* 2011-2746, 2011.
[37]Juve, D., Sunyach, M., and Comte-Bellot, G. , "Filtered Azimuthal Correlations in the Acoustic Far Field of a Subsonic Jet," *AIAA Journal*, Vol. 17, No. 1, 1979, pp. 112-113.
[38]Hileman, J. I., Thurow, B. S., Caraballo, E. J., and Samimy, M., "Large-scale structure evolution and sound emission in high-speed jets: real-time visualization with simultaneous acoustic measurements," *Journal of Fluid Mechanics*, Vol. 544, 2005, pp. 277-307.
[39]Cavalieri, A. V. G., Jordan, P., Gervais, Y., and Agarwal, A., "Jittering wave-packet models for subsonic jet noise," *AIAA/CEAS 16th Aeroacoustics Conference*, 2010-3957, 2010.
[40]Kearney-Fischer, M., Sinha, A., and Samimy, M., "Intermittent Nature of Subsonic Jet Noise," *AIAA Journal*, Vol. 51, No. 5, 2013, pp. 1142-1155.
[41]Torrence, C., and Compo, G. P., "A Practical Guide to Wavelet Analysis," *Bulletin of the American Meteorological Society*, Vol. 79, No. 1, 1998, pp. 61-78.

Downloaded by Mo Samimy on February 3, 2014 | http://arc.aiaa.org | DOI: 10.2514/6.2014-0527